

Tunable electric and magnetic resonances in multilayered metal/dielectric nanoplates at optical frequencies

De Li^{1,2}, Ling Qin¹, Dong-Xiang Qi¹, Feng Gao¹, Ru-Wen Peng^{1,3}, Jin Zou², Qian-Jin Wang¹ and Mu Wang¹

¹ National Laboratory of Solid State Microstructures and Department of Physics, Nanjing University, Nanjing 210093, People's Republic of China

² School of Engineering and Centre for Microscopy and Microanalysis, The University of Queensland, Brisbane, Qld 4072, Australia

E-mail: rwpeng@nju.edu.cn

Received 11 March 2010, in final form 22 June 2010

Published 9 August 2010

Online at stacks.iop.org/JPhysD/43/345102

Abstract

In this work, we investigate electromagnetic responses in multilayered Ag/SiO₂ nanoplates at optical frequencies. Electric and magnetic resonances, which originate from localized surface plasmons, are demonstrated by the effective permeability and permittivity, electric and magnetic field distributions, and measured transmission at oblique incidence. Furthermore, electric and magnetic resonances can be tailored by the geometrical parameters of the nanoplates. In a rectangular nanoplate, magnetic resonance only shifts with the width along the incident polarization, and electric resonance shifts obviously as the aspect ratio of the nanoplate changes. The investigation may provide a tunable building block for optical metamaterials.

(Some figures in this article are in colour only in the electronic version)

1. Introduction

Recently, negative-index metamaterials (NIMs) have attracted considerable attention because of a range of unprecedented electromagnetic properties that are unattainable from the materials in nature. In 1968, Veselago proposed the concept of negative refractive index or left-handed material [1] with both negative permittivity and negative permeability, and he predicted that such a material would have some unusual properties, for example, reversed Snell's law, Doppler shift and Cherenkov radiation. Negative permittivity is inherent to metallic materials, while negative permeability does not exist in naturally occurring materials, due to the lack of magnetic response above the gigahertz range. In 1999, Pendry *et al* proposed that magnetic resonance could be artificially achieved using an array of double split-ring resonators (SRRs) [2] made from nonmagnetic conducting materials. Later, Smith *et al* [3] demonstrated experimentally negative

permeability provided by SRRs and negative permittivity provided by the continuous conducting wires; they took the first step to demonstrate NIMs at microwave frequencies. Since then, the interest in NIMs has increased substantially and great efforts have been devoted to designing and fabricating NIMs from microwave to optical frequencies. At optical frequencies, magnetic response of SRRs [4–6] is saturated. Thereafter, many other subwavelength metallic structures that exhibit magnetic resonance have been investigated to obtain negative permeability, such as coupled metal nanostrips [7], the cut-metal wire pairs [8,9], nanorod pairs [10], gold nanosandwiches [11], fishnet structures [12] and so on. Metal–dielectric–metal sandwich is very common among these structures, while less attention has been paid to the multilayered metal/dielectric structures, such as nanodiscs of multiple metal layers [13]. Recently, a three-dimensional (3D) optical metamaterial with a negative refractive index has been realized in cascaded 'fishnet' structures [14]. 3D metamaterials are becoming increasingly attractive to achieve bulk properties such as the index of refraction.

³ Author to whom any correspondence should be addressed.

In this work, we investigate electromagnetic responses in multilayered Ag/SiO₂ nanoplates at optical frequencies. In multilayered nanoplates, there exist electric and magnetic responses, which originate from the coupling of localized surface plasmons (LSPs) on multiple Ag layers. We demonstrated the electric and magnetic resonances by the effective permeability and permittivity, the electric and magnetic field distributions and the measured transmission at oblique incidence. Then, we tailored electric and magnetic resonances by designing different geometrical parameters. It is found that in a rectangular nanoplate, the magnetic resonance only shifts with the width along the incident polarization, and the electric resonance shifts obviously as the aspect ratio of the nanoplate changes. Therefore, magnetic and electric resonances are tunable in multilayered metal/dielectric nanoplates.

2. Sample fabrication and optical measurement at normal incidence

Experimentally, the multilayered Ag/SiO₂ nanoplates were fabricated by magnetron sputtering and a focused-ion-beam (FIB) facility, and their optical spectra were measured by a microspectrophotometer. First, the multilayered Ag/SiO₂ films were coated on a piece of glass substrate by magnetron sputtering, then the arrays of nanoplates were fabricated on the films by a FIB facility (strata FIB 201, FEI company, 30 keV Ga ions). Figure 1(a) shows the field-emission scanning electronic microscope (SEM) image of the array of nanoplates, and the scale bar represents 200 nm. The periodicity of the lattices is about 400 nm and the widths of the nanoplate are about 165 nm along both axes. Figure 1(b) shows the transmission electron microscopy (TEM) image of cross section, and the scale bar represents 100 nm. The layer sequence from the glass substrate to the top is Ag/SiO₂/Ag/SiO₂/Ag/SiO₂/Ag/SiO₂ with a total thickness of 160 nm, where all Ag layers are 25 nm thick and SiO₂ layers are 13.3 nm thick, except that the topmost SiO₂ layer is 20 nm thick which protects the Ag layer below. Using a UV-visible-NIR microspectrophotometer (CRAIC QDI2010), the normal transmission spectrum of this sample was measured, as shown in figure 1(c). There are three dips in the transmission spectrum at wavelengths $\lambda = 494$ nm, 697 nm and 1041 nm, respectively. We will see that the transmission dip around $\lambda = 697$ nm originates from electric resonance, and the transmission dip around $\lambda = 1041$ nm originates from magnetic resonance.

3. Simulations and discussion

Numerical simulations are also performed to investigate the optical properties of the nanoplate array based on the full-vectorial three-dimensional finite-difference time-domain (FDTD) method [15]. In the simulations, this sample is modelled as a square array of the square nanoplates, with the periodicity of the lattice of 400 nm and the width of the nanoplate of 165 nm. And the frequency-dependent permittivity of Ag is obtained from the Lorentz-Drude model [16]. The calculated normal transmission spectrum in

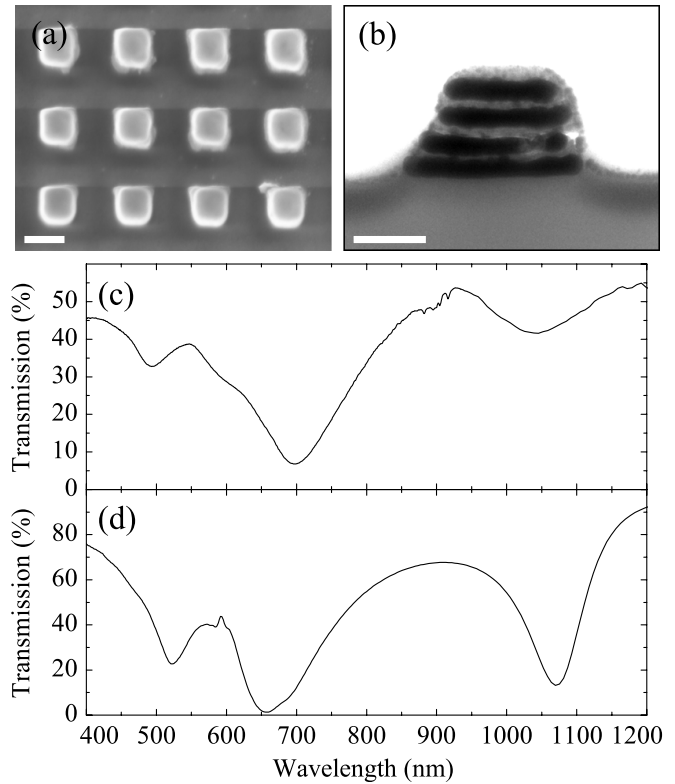


Figure 1. (a) The SEM image of the array of multilayered Ag/SiO₂ nanoplates on glass substrate, and the bar represents 200 nm. (b) The TEM image of the cross section of a nanoplate, where the layer sequence from the glass substrate to the top is Ag/SiO₂/Ag/SiO₂/Ag/SiO₂/Ag/SiO₂, and all Ag layers are 25 nm thick and SiO₂ layers are 13.3 nm thick except that the topmost SiO₂ layer is 20 nm thick. The bar represents 100 nm. The measured (c) and calculated (d) normal transmission spectra.

figure 1(d) has three dips at wavelengths $\lambda = 522$ nm, 657 nm and 1071 nm, respectively. It agrees with the experimental spectrum, except for a slight deviation in the position and the depth of these three dips. The deviation may come from the nonuniformity of the sample, the sidewall angle of the nanoplates, the roughness of the interfaces and the unevenness of the glass substrate, which have not been considered in the simulations.

From the numerical simulations, we have also extracted the effective permeability μ and permittivity ε of this sample, which would show us the underlying physics. We consider this sample as a homogeneous slab of 160 nm thickness between the glass substrate and air. The effective μ and ε along the in-plane axes of the nanoplates are derived from the normal reflection and transmission coefficients of the slab, analysed by a robust retrieval algorithm [17]. The retrieved effective μ and ε of this sample are plotted in figures 2(a) and (d), and the solid and dashed curves represent the real and imaginary parts, respectively (the same for all retrieved μ and ε). Around the wavelength $\lambda = 657$ nm, there is an evident drop in $\text{Re}(\varepsilon)$ and a big peak of $\text{Im}(\varepsilon)$, so an electric resonance occurs, which leads to negative $\text{Re}(\varepsilon)$ and the transmission dip at $\lambda = 657$ nm. While around the wavelength $\lambda = 1071$ nm, there is an evident drop in $\text{Re}(\mu)$ and a big peak of $\text{Im}(\mu)$, so a magnetic resonance occurs, which results in negative $\text{Re}(\mu)$ and the transmission

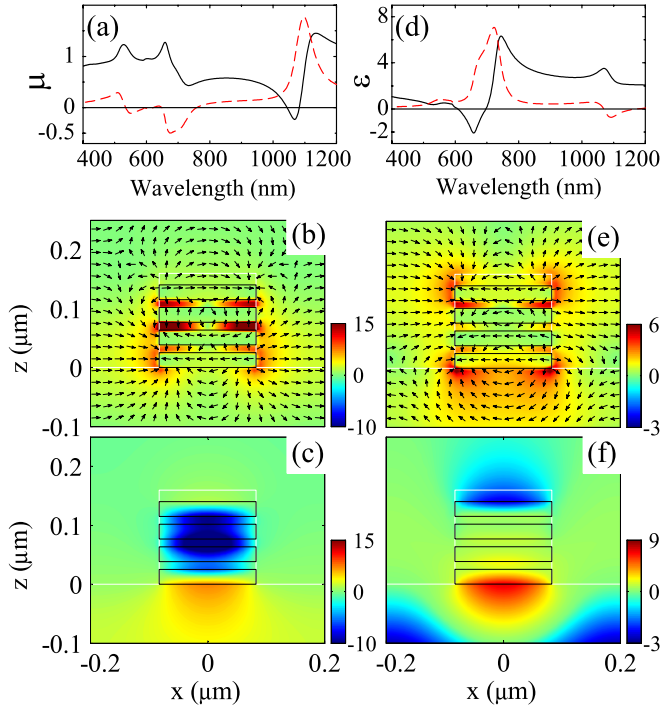


Figure 2. The retrieved permeability μ (a) and permittivity ε (d) for the sample described in figure 1(a), where the solid and dashed curves represent the real and imaginary parts, respectively (the same for all retrieved μ and ε). The x - z plane cross section of (b) the electric field distribution E where the arrows represent the direction and the colour map represents the intensity, and (c) the magnetic field distribution H_y along the y -axis at the magnetic resonance $\lambda = 1071$ nm. (e) and (f) are the field distributions at the electric resonance $\lambda = 657$ nm. Here, the incident light illuminates along the z -axis with x -polarization, and the black boxes and the white line represent Ag layers and the boundary of air, respectively.

dip at $\lambda = 1071$ nm. Around the wavelength $\lambda = 522$ nm, neither $\text{Re}(\varepsilon)$ nor $\text{Re}(\mu)$ is negative, and both $\text{Im}(\varepsilon)$ and $\text{Im}(\mu)$ are small, so the transmission dip may come from propagating surface plasmons.

To confirm the electric and magnetic resonances, we have calculated the electric and magnetic field distributions at wavelengths $\lambda = 657$ nm and $\lambda = 1071$ nm in this sample. Figures 2(b) and (c) illustrate the electric and magnetic field distributions, respectively, in the x - z plane at $\lambda = 1071$ nm. Here, the square nanoplate is in the x - y plane and its two axes are parallel to the x and y axes, respectively, and the incident light illuminates along the z -axis with x -polarization. It is shown that the electric fields in the upper and lower Ag layers are in the opposite directions, and in the SiO_2 layers, the electric fields are very strong with opposite directions between the left and right sides (as shown in figure 2(b)). Thus, the nanoplate can be viewed as an equivalent inductor-capacitor (LC) tank circuit, where the Ag layers play the role of inductors and the SiO_2 layers play that of capacitors. And a loop of the displacement current would be formed in the nanoplate. Figure 2(c) shows the magnetic field distribution H_y along the y -axis. The magnetic field at the centre of the nanoplate is quite strong, which can derive from the LC resonance. Because of the big net magnetic moment, this LC resonance is called as a magnetic resonance.

Figures 2(e) and (f) illustrate the electric and magnetic field distributions, respectively, in the x - z plane at $\lambda = 657$ nm. The electric fields in the upper and lower Ag layers are in the same directions, and the electric field around the four corners of the nanoplate is very strong, while that in the SiO_2 layers is weak (as shown in figure 2(e)). The magnetic field H_y at the centre of the nanoplate is weak while those at the top and bottom of the nanoplate are quite strong with opposite directions (as shown in figure 2(f)). Because of the big net electric moment, this resonance is called an electric resonance.

The electric and magnetic field distributions also reveal that the electric and magnetic resonances originate from the coupling of LSPs [18] on multiple Ag layers. The electric resonance corresponds to the in-phase coupling of the electric dipoles on multiple Ag layers, and the magnetic resonance corresponds to the out-of-phase coupling. Compared with the metal-dielectric-metal sandwiches [11], there are more metal layers in the multilayered Ag/ SiO_2 nanoplates, hence the physical process to generate the resonances is more complicated.

4. Dependence of the electric and magnetic resonances on incident angles

In order to illustrate experimentally the electric and magnetic resonances, we measured the transmission spectra of the sample at oblique incidence, where the incident angle θ varies from 0° up to 30° in steps of 5° . It is found that in transverse-electric (TE) incidence, when the incident angle θ increases, the electric resonance shifts to the red and its transmission dip becomes broader, while the magnetic resonance does not change (as shown in figure 3(a)). Meanwhile, in transverse-magnetic (TM) incidence, when the incident angle θ increases, the electric resonance shifts to the red, while the magnetic resonance does not change (as shown in figure 3(b)). Therefore, for both polarizations, the electric resonance shifts to the red as the incident angle θ increases, while the magnetic resonance does not. Actually, when the incident angle θ increases, the phase differences between the moments of the induced electric or magnetic dipoles will increase [19]. For the electric resonance, both the electric and magnetic fields are very strong outside the nanoplates (as shown in figures 2(e) and (f)), hence the coupling between the adjacent nanoplates is very strong, which will be affected by the phase differences. As a result, the electric resonance will shift to the red. While for the magnetic resonance, both the electric and magnetic fields are located inside the nanoplates (as shown in figures 2(b) and (c)), hence the coupling between the adjacent nanoplates is very weak. Therefore, the magnetic resonance will hardly be affected by the phase differences, and the resonant wavelength will not increase with the incident angle θ .

In addition, for TM incidence, an additional transmission dip occurs around $\lambda = 600$ nm, and it deepens and shifts to the red as the incident angle θ increases. This transmission dip may be related to the out-of-plane component of the electric field E_z of the incident light. Actually in the nanoplates, some electric dipoles are induced by E_z , then they couple to each other in the array and form a resonance mode. When the incident

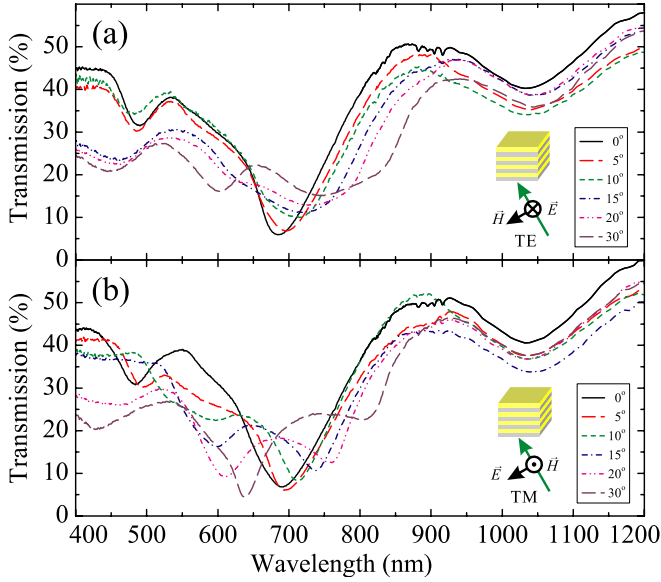


Figure 3. The measured transmission spectra of the sample described in figure 1(a) for TE (a) and TM (b) incidence with incident angles $\theta = 0^\circ, 5^\circ, 10^\circ, 15^\circ, 20^\circ$ and 30° . The insets in (a) and (b) show the configurations of TE and TM incidence, respectively.

angle θ increases, the phase differences between the moments of induced electric dipoles will increase, hence the coupled resonance mode will shift to the red. While for TE incidence, an additional dip occurs around $\lambda = 600$ nm for $\theta = 30^\circ$, which is related to the out-of-plane component of the magnetic field H_z of the incident light.

5. Tune the electric and magnetic resonances

Due to the fact that electric and magnetic resonances in multilayered nanoplates originate from LSPs, it is possible to tune these two resonances by changing the geometrical parameters [20] in multilayered nanoplates. Figure 4(a) shows the configuration of normal incidence on an array of rectangular nanoplates, and the incident light illuminates along the z -axis with x -polarization. In the following numerical simulations, we vary the width u_x parallel to the incident polarization and the other width u_y of the rectangular nanoplates, in order to tailor the electric and magnetic resonances. In these cases, we keep the periodicities of the lattice, $a_x = a_y = 400$ nm, the layer sequence and thickness of the nanoplates as the sample in figure 1(a).

We start from the square nanoplates and investigate the electric and magnetic resonances with varying width of the nanoplate. Figure 4(b) shows the transmission spectra for the width from 145 to 185 nm. As the width of the square nanoplate increases, the magnetic resonance (the transmission dip at long wavelength) shifts to the red obviously, while the electric resonance (the transmission dip around $\lambda = 657$ nm) just shifts a little bit to the red. The retrieved effective permeability μ and permittivity ϵ (shown in figures 4(c) and (d)) confirm the magnetic and electric resonances, respectively. Following the magnetic resonance, negative $\text{Re}(\mu)$ dramatically shifts to the

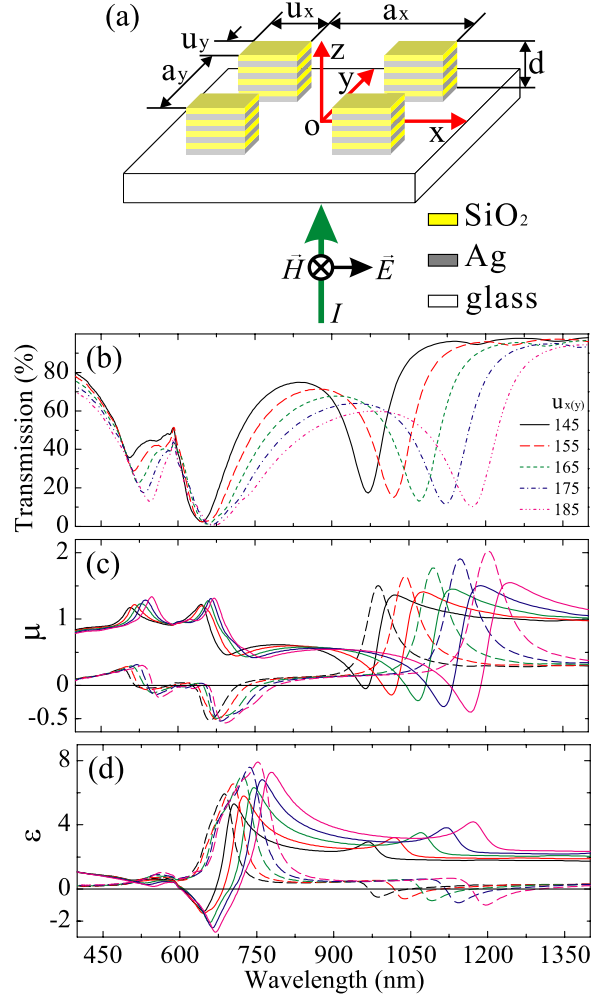


Figure 4. (a) The configuration of the normal incidence on the array of rectangular nanoplates, and the incident light illuminates along the z -axis with x -polarization. The calculated normal transmission spectra (b), the retrieved permeability μ (c) and permittivity ϵ (d) for square nanoplates with widths $u_x = u_y = 145, 155, 165, 175$ and 185 nm.

red when the width of the nanoplate increases, but negative $\text{Re}(\epsilon)$ shifts only slightly.

Now we come to the rectangular nanoplates with varying two widths u_x and u_y , respectively, in order to see the dependence of the electric and magnetic resonances on each of the widths. First, we tune the width u_x (as shown in figure 4(a)) from 145 to 185 nm, which is parallel to the incident polarization, and keep $u_y = 165$ nm. In the transmission spectra shown in figure 5(a), as the width u_x increases, the magnetic resonance (the transmission dip at long wavelength) shifts to the red, and the electric resonance (the transmission dip around $\lambda = 657$ nm) shifts slightly to the red. The result is confirmed by the retrieved permeability μ and permittivity ϵ (as shown in figures 5(b) and (c)). As u_x increases, negative $\text{Re}(\mu)$ shifts to the red, while negative $\text{Re}(\epsilon)$ just shifts a little. Second, we tune the width u_y from 145 to 185 nm, which is perpendicular to the incident polarization, and keep $u_x = 165$ nm. As u_y increases, the magnetic resonance does not shift and the electric resonance shifts slightly to the blue (as shown in figure 5(d)). Correspondingly,

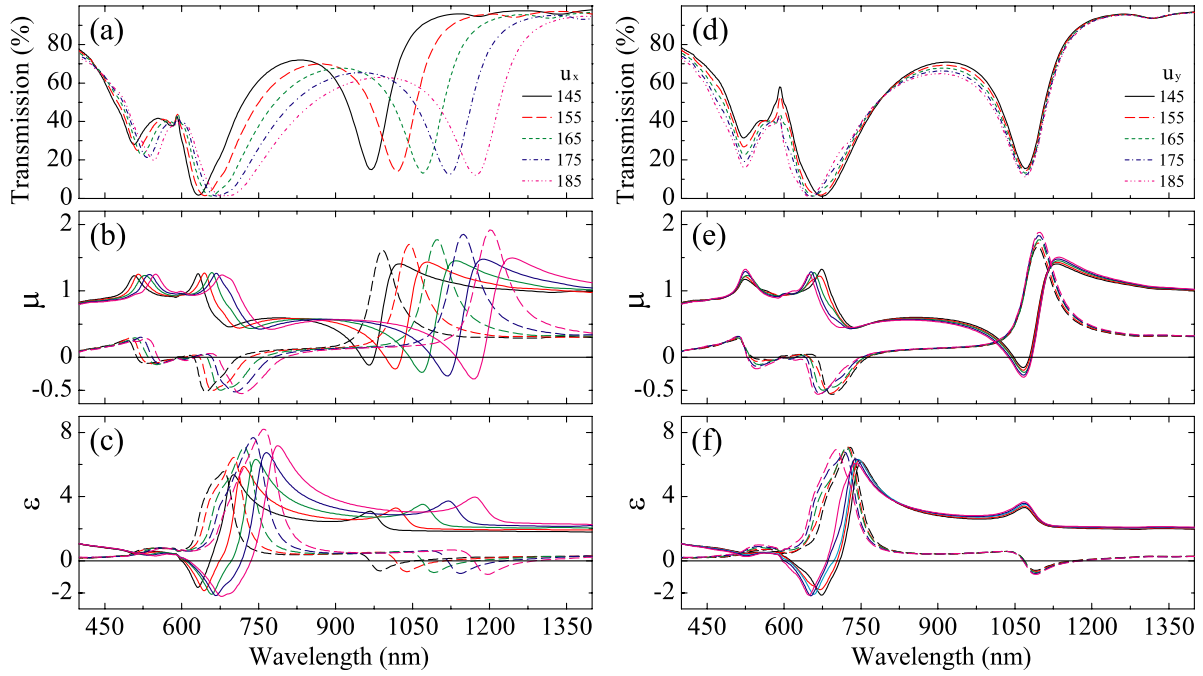


Figure 5. The calculated normal transmission spectra (a), the retrieved permeability μ (b) and permittivity ϵ (c) for rectangular nanoplates with widths $u_x = 145, 155, 165, 175$ and 185 nm parallel to the incident polarization, and the other width $u_y = 165$ nm. (d), (e) and (f) for rectangular nanoplates with widths $u_y = 145, 155, 165, 175$ and 185 nm perpendicular to the incident polarization, and the other width $u_x = 165$ nm.

negative $\text{Re}(\mu)$ does not shift either and negative $\text{Re}(\epsilon)$ also shifts to the blue (as shown in figures 5(e) and (f)). Therefore, we show that in the case that the incident polarization is parallel to u_x of the nanoplate, the magnetic resonance dramatically shifts to the red and the electric resonance shifts slightly to the red when the width u_x increases; in contrast, both the electric and magnetic resonances almost do not shift when the width u_y increases.

Furthermore, we tune the aspect ratio u_x/u_y of the rectangular nanoplates to tailor the electric and magnetic resonances, where the width u_x (u_y) is parallel (perpendicular) to the incident polarization. The transmission spectra for the aspect ratio u_x/u_y from 145/185 to 185/145 are shown in figure 6(a). Interestingly, the electric resonance (the transmission dip around $\lambda = 657$ nm) shifts to the red obviously, meanwhile, the magnetic resonance (the transmission dip at long wavelength) shifts to the red dramatically. The retrieved permeability μ and permittivity ϵ in figures 6(b) and (c) also show that negative $\text{Re}(\epsilon)$ shifts with the aspect ratio u_x/u_y obviously and negative $\text{Re}(\mu)$ shifts dramatically. Therefore, both the electric and magnetic resonances can be tailored evidently by the aspect ratio of the nanoplate.

Generally, in rectangular nanoplates, the magnetic resonance can be tailored to the red by changing the width u_x parallel to the incident polarization, and the electric resonance can be tailored obviously by the aspect ratio u_x/u_y . As a consequence, the permeability μ and permittivity ϵ are tunable in the multilayered nanoplates. Actually, we have demonstrated that the electric and magnetic resonances can be tailored by changing the geometrical parameters in multilayered nanoplates.

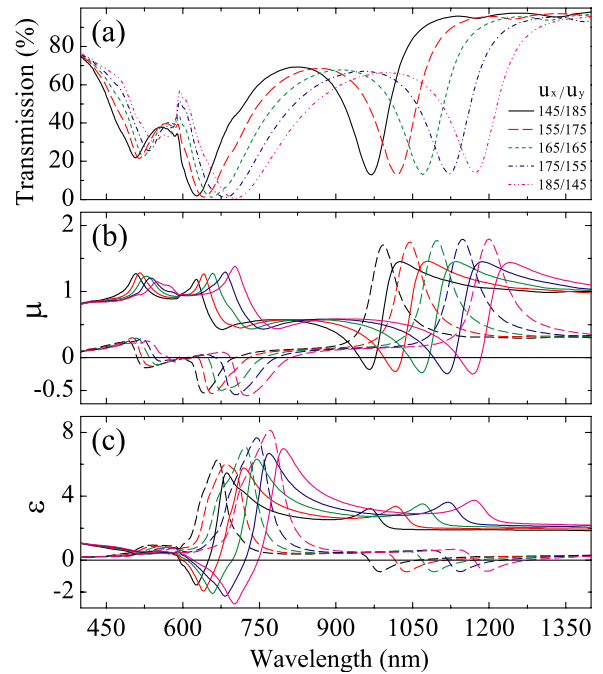


Figure 6. The calculated normal transmission spectra (a), the retrieved permeability μ (b) and permittivity ϵ (c) for rectangular nanoplates with aspect ratios $u_x/u_y = 145/185, 155/175, 165/165, 175/155$ and 185 nm/145 nm, where the width u_x (u_y) is parallel (perpendicular) to the incident polarization.

In addition, we investigate the influence of lattice periodicities on the electric and magnetic resonances in the nanoplate arrays. Here, we keep the widths of the square nanoplates to be $u_x = u_y = 165$ nm, and keep the layer sequence and thickness of the nanoplates the same as those

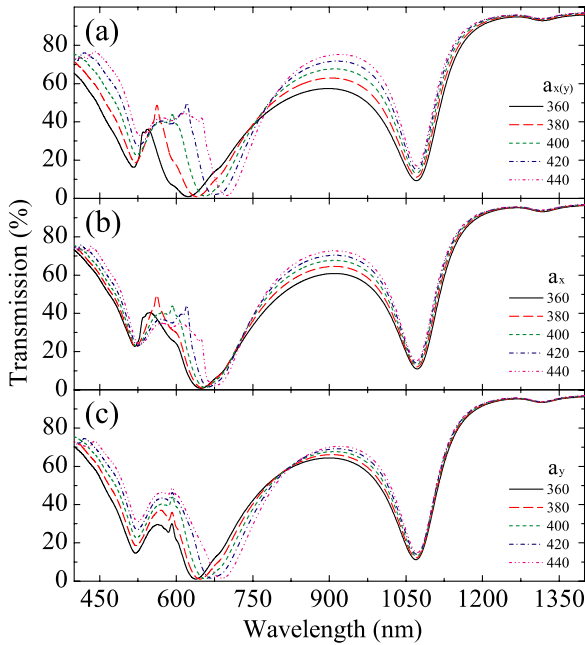


Figure 7. The calculated normal transmission spectra for square nanoplates with periodicities (a) $a_x = a_y = 360, 380, 400, 420$ and 440 nm, (b) $a_x = 360, 380, 400, 420$ and 440 nm and $a_y = 400$ nm, and (c) $a_y = 360, 380, 400, 420$ and 440 nm and $a_x = 400$ nm, where the periodicity a_x (a_y) is parallel (perpendicular) to the incident polarization. Here, the width of the square nanoplates is 165 nm, and the layer sequence and thickness of the nanoplates are the same as those in figure 1(a).

in figure 1(a). As to the square array, when the periodicities of the nanoplates vary from 360 to 440 nm, the electric resonance (the transmission dip around $\lambda = 657$ nm) shifts to the red obviously, while the magnetic resonance (the transmission dip at long wavelength) hardly shifts, as shown in figure 7(a). For the electric resonance, both the electric and magnetic fields are very strong outside the nanoplates (as shown in figures 2(e) and (f)), hence the interactions between adjacent polarized nanoplates are very strong. As the distances between the nanoplates increase, the interaction varies and the electric resonance shifts to the red. In contrast, for the magnetic resonance, both the electric and magnetic fields are located inside the nanoplates (as shown in figures 2(b) and (c)), and the interaction between adjacent polarized nanoplates is very weak. Therefore, the magnetic resonance does not shift as the periodicities increase.

Actually, the increase in both periodicities a_x and a_y contributes to the redshift of the electric resonance, as shown in figures 7(b) and (c), where a_x and a_y are parallel and perpendicular to the incident polarization, respectively. When the periodicity a_x varies from 360 to 440 nm and a_y remains as 400 nm, the electric resonance shifts slightly to the red, as shown in figure 7(b). In this case, the diffraction light at grazing angle along the x -axis in the glass substrate, which leads to a strong interaction between adjacent polarized nanoplates, is modified by wavelength $\lambda = n_{\text{glass}} \cdot a_x$ (n_{glass} is the refractive index of glass), hence the electric resonance is pushed to the red. Meanwhile, when the periodicity a_y varies from 360 to 440 nm and a_x remains as 400 nm, the

electric resonance shifts obviously to the red, as shown in figure 7(c). As the distances between the nanoplates along the y -axis increases, their interactions are modified, which gives rise to the redshift of the electric resonance. As a result, the electric resonance can also be tailored by the periodicities of the nanoplate array.

6. Conclusions

In conclusion, we have investigated the optical properties of multilayered Ag/SiO₂ nanoplates by both experiments and numerical simulations. The sample was fabricated using magnetron sputtering and a FIB facility, and its transmission spectra were measured by a microspectrophotometer. Numerical simulations based on the full-vectorial three-dimensional FDTD method were performed. The electric and magnetic resonances are demonstrated in the multilayered Ag/SiO₂ nanoplates by the effective permeability and permittivity, the electric and magnetic field distributions, and the measured transmission at oblique incidence. The electric and magnetic resonances are tuned by the geometrical parameters of the multilayered nanoplates. In a rectangular nanoplate, the magnetic resonance only shifts with the width along the incident polarization, and the electric resonance shifts obviously as the aspect ratio of the nanoplate changes. In addition, the electric resonance can also be tailored by the periodicity of the nanoplate array. The investigation may provide a tunable building block for optical metamaterials.

Acknowledgments

This work was supported by grants from the National Natural Science Foundation of China (Grant Nos 10625417, 50972057 and 10874068), the State Key Programme for Basic Research from the Ministry of Science and Technology of China (Grant Nos 2010CB630705 and 2006CB921804) and partly by the Jiangsu Province (Grant No BK2008012).

References

- [1] Veselago V G 1968 The electrodynamics of substances with simultaneously negative values of ϵ and μ *Sov. Phys.—Usp.* **10** 509–14
- [2] Pendry J B, Holden A J, Robbins D J and Stewart W J 1999 Magnetism from conductors and enhanced nonlinear phenomena *IEEE Trans. Microw. Theory Tech.* **47** 2075–84
- [3] Smith D R, Padilla W J, Vier D C, Nemat-Nasser S C and Schultz S 2000 Composite medium with simultaneously negative permeability and permittivity *Phys. Rev. Lett.* **84** 4184–7
- [4] Yen T J, Padilla W J, Fang N, Vier D C, Smith D R, Pendry J B, Basov D N and Zhang X 2004 Terahertz magnetic response from artificial materials *Science* **303** 1494–6
- [5] Linden S, Enkrich C, Wegener M, Zhou J, Koschny T and Soukoulis C M 2004 Magnetic response of metamaterials at 100 terahertz *Science* **306** 1351–3
- [6] Xiong X, Sun W H, Bao Y J, Peng R W, Wang M, Sun C, Lu X, Shao J, Li Z F and Ming N B 2009 Switching the electric and magnetic responses in a metamaterial *Phys. Rev. B* **80** 201105(R)

- [7] Yuan H K, Chettiar U K, Cai W S, Kildishev A V, Boltasseva A, Drachev V P and Shalaev V M 2007 A negative permeability material at red light *Opt. Express* **15** 1076–83
- [8] Dolling G, Enkrich C, Wegener M, Zhou J F, Soukoulis C M and Linden S 2005 Cut-wire pairs and plate pairs as magnetic atoms for optical metamaterials *Opt. Lett.* **30** 3198–200
- [9] Pshenay-Severin E, Hübner U, Menzel C, Helgert C, Chipouline A, Rockstuhl C, Tünnermann A, Lederer F and Pertsch T 2009 Double-element metamaterial with negative index at near-infrared wavelengths *Opt. Lett.* **34** 1678–80
- [10] Shalaev V M, Cai W S, Chettiar U K, Yuan H K, Sarychev A K, Drachev V P and Kildishev A V 2005 Negative index of refraction in optical metamaterials *Opt. Lett.* **30** 3356–8
- [11] Pakizeh T, Abrishamian M S, Granpayeh N, Dmitriev A and Käll M 2006 Magnetic-field enhancement in gold nanosandwiches *Opt. Express* **14** 8240–6
- [12] Zhang S, Fan W J, Panoiu N C, Malloy K J, Osgood R M and Brueck S R J 2005 Experimental demonstration of near-infrared negative-index metamaterials *Phys. Rev. Lett.* **95** 137404
- [13] Su K H, Wei Q H and Zhang X 2006 Tunable and augmented plasmon resonances of Au/SiO₂/Au nanodisks *Appl. Phys. Lett.* **88** 063118
- [14] Valentine J, Zhang S, Zentgraf T, Ulin-Avila E, Genov D A, Bartal G and Zhang X 2008 Three-dimensional optical metamaterial with a negative refractive index *Nature* **455** 376–9
- [15] Taflove A and Hagness S C 2005 *Computational Electrodynamics: The Finite-Difference Time-Domain Method* 3rd edn (Norwood: Artech House)
- [16] Rakic A D, Djuricic A B, Elazar J M and Majewski M L 1998 Optical properties of metallic films for vertical-cavity optoelectronic devices *Appl. Opt.* **37** 5271–83
- [17] Smith D R, Schultz S, Markoš P and Soukoulis C M 2002 Determination of effective permittivity and permeability of metamaterials from reflection and transmission coefficients *Phys. Rev. B* **65** 195104
- [18] Bao Y J, Peng R W, Shu D J, Wang M, Lu X, Shao J, Lu W and Ming N B 2008 Role of interference between localized and propagating surface waves on the extraordinary optical transmission through a subwavelength-aperture array *Phys. Rev. Lett.* **101** 087401
- [19] Zhang Z J, Peng R W, Wang Z, Gao F, Huang X R, Sun W H, Wang Q J and Wang M 2008 Plasmonic antenna array at optical frequency made by nanoapertures *Appl. Phys. Lett.* **93** 171110
- [20] Wu S, Wang G D, Wang Q J, Zhou L, Zhao J W, Huang C P and Zhu Y Y 2009 Novel optical transmission property of metal–dielectric multilayered structure *J. Phys. D: Appl. Phys.* **42** 225406